Strain-induced phase separation in La$_{0.7}$Sr$_{0.3}$MnO$_3$ thin films

A. Tebano, C. Aruta,[*] P. G. Medaglia, F. Tozzi, and G. Balestrino

CNR-INFM Coherentia and Dipartimento di Ingegneria Meccanica, Universita' di Roma Tor Vergata, Via del Politecnico 1,
I-00133 Roma, Italy

A. A. Sidorenko, G. Allodi, and R. De Renzi

Dipartimento di Fisica and Unita' CNISM di Parma, Via G.P. Usberti 7A, I-43100 Parma, Italy

G. Ghiringhelli, C. Dallera, and L. Braicovich

CNR-INFM Coherentia and Soft, Dipartimento di Fisica, Politecnico di Milano, piazza Leonardo da Vinci 32, I-20133 Milano, Italy

N. B. Brookes

European Synchrotron Radiation Facility, Boîte Postal 220, 38043 Grenoble, France

La$_{0.7}$Sr$_{0.3}$MnO$_3$ thin films having different thicknesses were grown by pulsed laser deposition with *in situ* reflection high energy electron diffraction diagnostics on LaAlO$_3$ substrates. The mismatch between film and substrate gives rise to an in-plane compressive biaxial strain, which partially relaxes in films thicker than 30 unit cells. Accordingly, the ratio between the out-of-plane and the in-plane lattice parameter (c/a) varies between 1.06 (fully strained) and 1.03 (partially relaxed). In-plane compressive strain favors the stabilization of the $3z^2-r^2$ orbitals (chain-type antiferromagnetic phase), thus giving rise to a sizeable x-ray absorption linear dichroism signal. The shape of the linear dichroism depends weakly on the c/a ratio, while its intensity strongly increases with c/a. At the same time, the metal-insulator transition temperature shifts from about 360 K towards lower temperatures with decreasing thickness, eventually reaching an insulating state for the 30 unit cells film. Low-temperature nuclear magnetic resonance spectra show a decrease of the Mn^{DE} double-exchange metallic contribution with decreasing the thickness, which becomes negligible in the 30 unit cells thick film. The experimental results demonstrate a strain driven competition between two stable phases: the orbital ordered chain-type insulating antiferromagnetic and the orbital disordered metallic ferromagnetic. For intermediate values of the epitaxial strain the local minimum state of the system lies in a gap region between the two stable phases. Such a region has glassy characteristics with coexisting clusters of the two phases. The strain is used as a driving force to span the glassy region.

I. INTRODUCTION

Mixed valence manganites $R_{1-x}A_x$MnO$_3$ (where R stands for rare earth and A for alkaline earth) show an extremely rich variety of noticeable physical properties. Such a complex behavior is thought to be a consequence of the interplay among several physical degrees of freedom (such as spin, charge, lattice, and orbital) simultaneously active in these materials.[1,2] As a consequence, after more than fifty years from the discovery of this class of materials, some fundamental aspects of their physical behavior are not yet fully understood.[1] In particular, the intrinsic inhomogeneous behavior of manganites with phase separation phenomena occurring on a nanometer scale has recently attracted increasing attention. Such phenomena are thought to be a consequence of the competition among nearly degenerate phases in the presence of sizeable quenched disorder arising, for instance, from cation substitution, oxygen deficiency or inhomogeneous strain.[2] In this scenario phenomena such as the appearance of glassy regions of mixed phases which show up at a critical temperature T^* above the ferromagnetic/antiferromagnetic ordering temperatures occur.[3,4] Phase separation has been experimentally investigated by space resolved techniques such as scanning tunnel microscopy,[5] magnetic force microscopy,[6] and electron transmission microscopy[7] which have shown a nanometric network of conducting/insulating (magnetic/nonmagnetic) domains. The interest toward phase separation phenomena is further motivated by its interplay with colossal magnetoresistance phenomena.[8]

The complex phase diagram of mixed valence manganites is currently spanned by varying temperature, chemical composition, carrier concentration, and by applying external magnetic or electric fields. One approach consists of controlling the manganite phase diagram by epitaxial strain induced in thin manganite films by mismatched substrates. Such an approach has the advantage of not varying the chemistry nor the carrier content of the manganite film. Namely, it has been reported that, in manganite thin films, epitaxial strain can give rise to different orbital orderings, such as layer-type antiferromagnetic (A) and chain-type antiferromagnetic (C).[9] Epitaxial biaxial strain ($\varepsilon_{xx}=\varepsilon_{yy}\neq\varepsilon_{zz}$) couples with the orbital degree of freedom via the distortion of the MnO$_6$ octahedra.[10] Depending on the octahedral distortion, if in-plane compressive or tensile, epitaxial strain favors the $3z^2-r^2$ (C-type antiferromagnetic) or the x^2-y^2 (A-type antiferromagnetic) orbital ordering, respectively. Recently, such an effect was experimentally observed in La$_{0.7}$Sr$_{0.3}$MnO$_3$ (LSMO) thin films grown on LaAlO$_3$ and SrTiO$_3$ substrates.[11] In this paper we investigate LSMO thin films,

having different thickness, grown on (100) LaAlO$_3$ (LAO) substrates. The crystal structure of bulk LSMO is rhombohedral with a pseudocubic lattice parameter of a_{LSMO} = $a_{rhomb}/\sqrt{2} \sim 3.87$ Å and the LAO substrate is rhombohedral with a pseudocubic lattice parameter of a_{LAO} = 3.786 Å. Mismatched cubic LAO substrates, (100) oriented, induce a tetragonal distortion in epitaxial thin films which increases the length of the perpendicular c lattice parameter of LSMO films (compressive in-plane strain). In case of ideal epitaxial growth the in-plane compressive strain will be

$$\varepsilon_{\parallel} = \frac{a_{LAO} - a_{LSMO}}{a_{LAO}} = -2.2 \% .$$

In thicker films the epitaxial strain can undergo partial relaxation relative to the value quoted above. Therefore, the strain state of LSMO films can be varied by varying the film thickness.

To study the strain induced orbital ordering in LSMO films, we have carried out linear dichroism (LD) in x-ray absorption spectroscopy (XAS) at Mn 2p-edge (dominant photon-excited transition $2p \rightarrow 3d$), because it directly probes the orbital character of $3d$ states in manganites.[12] On the other hand, we have performed zero-field ^{55}Mn nuclear magnetic resonance (NMR) to investigate directly the valence state of Mn ions.[13,14] Because electronic and magnetic properties arise from the Mn 3d electrons, comparison between XAS-LD and NMR spectra can be a tool of primary importance to understand the effect of biaxial strain on the electronic properties of manganites.

II. EXPERIMENT

Manganite films were grown by pulsed laser deposition (PLD) with *in situ* reflection high energy electron diffraction (RHEED) diagnostics. Oscillations of the RHEED diffraction spots were used to calibrate film thickness at the level of a single unit cell. Film deposition was carried out using an excimer laser charged with KrF (248 nm wavelength, pulse width 25 ns). The laser beam, with an energy per pulse of about 1 mJ, was focused onto a target with an energy density per laser pulse of about 0.1 J/cm^2. The background atmosphere consisted of a mixture of O$_2$ with 10% ozone. The average background pressure in the chamber was about 10^{-4} mbar and the substrate temperature 650 °C. Such a low background pressure is necessary in order to allow the *in situ* use of RHEED. On the other hand, a critical issue in the growth of manganite films is the oxygen deficiency which can arise from the reduced background pressure. Such a deficiency can strongly affect physical properties of manganite films. In most cases, in order to achieve full oxidation, manganite films undergo a high temperature post-annealing treatment. However, such a treatment can result in a partial film regrowth which deteriorates the film structural properties. Recently, we have developed an approach which allows one to grow fully oxidized manganite films by low-pressure PLD with *in situ* RHEED. Details about this technique are given in Ref. 15.

Film structural properties were investigated by x-ray diffraction measurements (XRD) at Cu $K\alpha$ wavelength in the
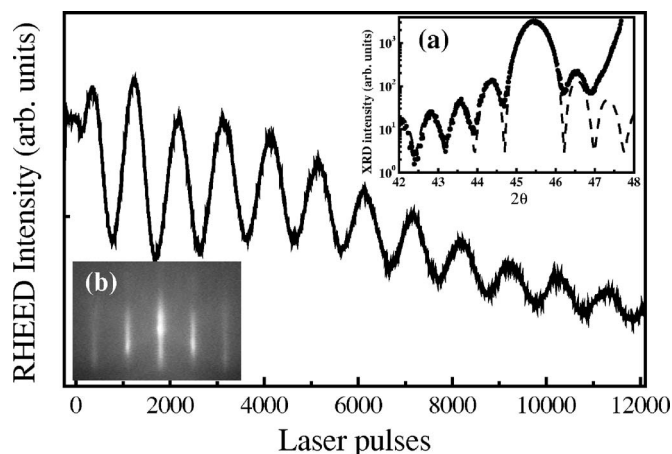

FIG. 1. Intensity oscillations of the RHEED specular spot at the first stage of the film growth. In the inset (a) the (002) XRD peak of the 30 u.c. film is shown. Well-defined finite size oscillations can be noticed on both sides of the main peak: the dashed line represents the simulated behavior for a 30 u.c. thick film. In the inset (b) the RHEED diffraction pattern at the end of the film growth is shown (30 u.c. thick film).

Bragg-Brentano configuration. Measurements were performed both in symmetrical and asymmetrical configurations to obtain the out-of-plane and in-plane lattice parameters, respectively. Electrical transport measurements were carried out by the standard four-probe technique as a function of temperature. XAS measurements were performed at the ID08 beam line of the European Synchrotron Radiation Facility (ESRF).[16] In order to measure XAS-LD, the linear polarization direction of the x-ray incident beam was rotated from horizontal (H) to vertical (V). XAS spectra were recorded by collecting the sample drain current. Low-temperature ^{55}Mn NMR spectra were collected with the home-built phase coherent spectrometer HyReSpect[17] by a solid spin echo sequence on a tuned probe circuit. The amplitude is recorded at each frequency to obtain the zero frequency component of the fast Fourier transform of the echo.

III. RESULTS

LSMO films were grown with thickness ranged from 100 unit cells to 30 unit cells (u.c.). Thickness was controlled with a precision of a single unit cell monitoring *in situ* the oscillations of the RHEED specular spot. Figure 1 shows the RHEED intensity oscillations during the initial stage of film deposition. From these oscillations a deposition rate of about 10^{-3} u.c./laser pulse was calculated. Moreover, the film thickness was also measured *a posteriori* by the finite size oscillations of the (002) x-ray diffraction peak [inset (a) in Fig. 1]. The latter estimate agreed, within one unit cell, with the value obtained counting the RHEED intensity oscillations. The layer-by-layer nature of the growth process was proved by the RHEED diffraction pattern at the end of the growth, which showed typical 2D features [inset (b) in Fig. 1].

Epitaxial LSMO films deposited on (100) LAO substrates are under compressive strain with $\epsilon = -2.2\%$. Strained layers
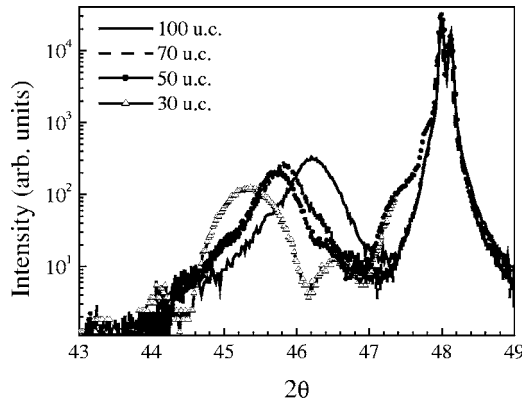
FIG. 2. (002) XRD symmetric reflections for the LSMO films of different thickness. The strong diffraction peak at 2Θ about 48° comes from the LAO substrate.

start to relax upon reaching a critical thickness t_c, whose value depends both on the mismatch between film and substrate and on the film growth conditions. We found that our LSMO films grown on LAO substrates start to relax above 30 u.c., in rough agreement with typical t_c values reported in literature.[18] Strain relaxation was carefully monitored by both symmetric and asymmetric XRD measurements. In Fig. 2 we show the symmetric Θ-2Θ measurements around the (002) reflection for LSMO films having different thickness. A gradual shift of the peak position toward higher angles (smaller perpendicular lattice parameters) can be noticed as the film thickness is increased from 30 to 100 u.c. This finding is indicative of a partial strain relaxation as the film thickness is increased. The ratio between the out-of-plane c lattice parameter and the in-plane a lattice parameter [estimated by Lorentzian fit of the (103) asymmetric reflection] results to be 1.06, 1.045, 1.04, and 1.03, for films having a thickness of 30, 50, 70, and 100 u.c., respectively. The reciprocal space maps of the asymmetric (103) reflection are reported in Fig. 3 for the same set of films. In the case of the 30 u.c. thick film, the diffraction peaks from film and substrate show the same in-plane scattering vector, as expected in the case of perfect in-plane matching between film and substrate. On the contrary, the out-of-plane scattering vectors are quite different, in agreement with the elastic elongation of the out-of-plane lattice constant c. According to the continuum elasticity theory, the in-plane strain is related to the perpendicular strain by the expression

$$\frac{\Delta c}{c} = -\frac{2\nu}{1-\nu}\frac{\Delta a}{a},$$

where ν is the Poisson's ratio, Δa and Δc the lattice parameter variation relative to the bulk values in-plane and out-of-plane, respectively. The Poisson's ratio ν, estimated from the experimental values of Δa and Δc for the fully strained film, is about 0.40. In the same figure the expected peak positions for a fully relaxed film and a fully strained film are indicated by an asterisk. The line joining the two asterisks represents the strain relaxation line in the reciprocal space. A partial strain relaxation in thicker films is confirmed by the increase of the XRD intensity along the relaxation line. Resistance
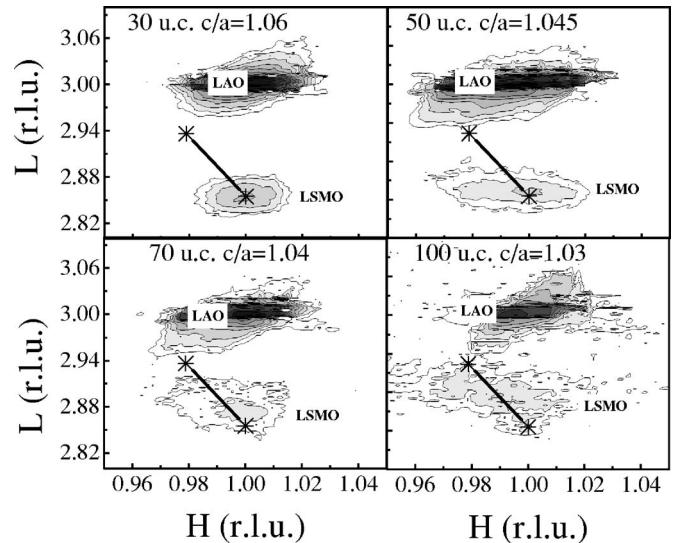

FIG. 3. Asymmetric XRD maps around the (103) peak for the four films having different thickness. Asterisks indicate the expected positions for the fully strained and fully relaxed LSMO films. The full line joining the two asterisks represents the film relaxation line.

measurements as a function of the temperature are reported in Fig. 4. The 100 u.c. thick film has a maximum of resistivity above 360 K, in agreement with values found for bulk LSMO samples. Samples with thickness of 70 and 50 u.c. show a metal-insulator transition at T_P temperatures of 275 and 250 K, respectively. On the contrary, the thinnest LSMO film (30 u.c. thick) shows an insulating behavior over the whole temperature range.

The same LSMO films of different thickness were investigated by XAS-LD at the $L_{2,3}$ edges. The results are reported in Fig. 5. Details about data treatment are given in Ref. 11. In the case of a ferromagnetic metallic unstrained LSMO sample, no LD signal is expected, because of the orbital disordered state. On the contrary, the experimental spectra of our epitaxial films (Fig. 5) show a clear LD signal. It can be observed that, while the shape of the LD spectra remains essentially unchanged, the relative LD signal intensity (in percent of the XAS L_3 peak height signal) increases notice-
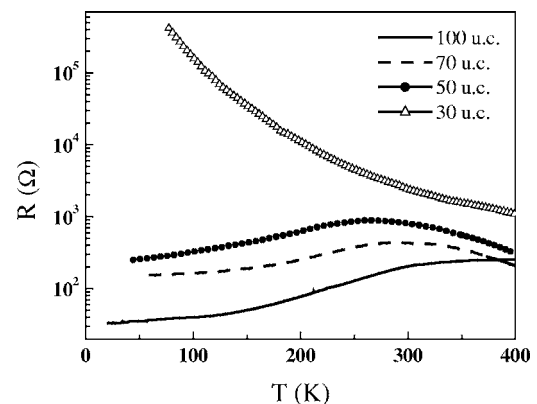

FIG. 4. Resistance versus temperature behavior for the four LSMO films on LAO substrates investigated in this paper.
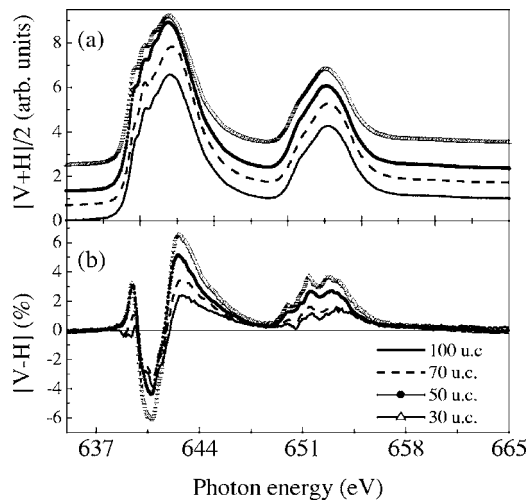
FIG. 5. Experimental XAS and LD for the four films having different thickness: (a) average between experimental XAS signals taken in V and H polarizations $(V+H)/2$, offset for clarity; (b) LD=$V-H$ in percent of the absorption shown in panel (a).

ably for thinner films. In Fig. 6 we also report the theoretical calculations with the Cowan's Hartree-Fock atomic code,[19] assuming an in-plane compressive $(c/a>1)$ tetragonal distortion and using a single $3d^4$ configuration (Mn^{3+}). The $3d$ levels splitting induced by the tetragonal distortion is parametrized by Ds and Dt, as shown in the top panel of Fig. 6. The comparison between the experimental and calculated spectra reported in Fig. 6 shows a satisfactory qualitative agreement. Further details concerning calculations are given in Ref. 11, where it was found that the shape and the intensity of calculated LD spectra are not very sensitive to variations of the microscopic crystal field parameters. On the other hand, panel (c) of Fig. 6 indicates that the intensity of the LD is much smaller in the experimental than in the theoretical spectra. As already stated in Ref. 11 we attribute this noticeable discrepancy to two facts. First, in our samples the F phase is anyway present: this phase is metallic and should not give LD, as no preferential orientation of the occupied orbitals at the Mn sites should be present. Second, our simplified calculations do not take into account the Mn^{4+} sites, that should also give a much reduced LD due to their quasi-spherical $3d$ electron spatial distribution. That is why, in the following discussion, we concentrate our attention on the shape of the LD and on the relative amplitude in the experimental data, not on its absolute size.

Finally we have recorded zero applied field ^{55}Mn NMR spectra on the same films. In mixed valence manganites different Mn states give rise to different contributions which can be easily distinguished in the NMR spectra reported in Fig. 7.

First of all the radio frequency power of the NMR excitation pulses was optimized for maximum signal intensity at the peak positions in the spectrum. Very low power was required (typically 35 dB below standard condition for nonmagnetic Mn nuclei), indicating a large ferromagnetic enhancement.[13,14] This means that all detected nuclei belong to a ferromagnetic environment. Localized Mn^{4+} states result in a peak between 310 and 330 MHz. The Mn^{DE} double ex-
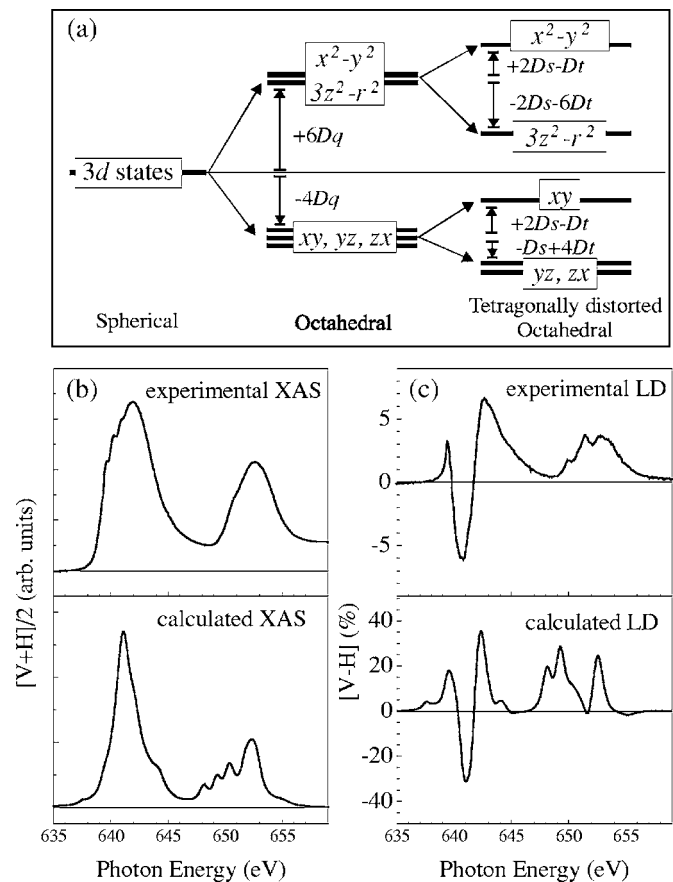

FIG. 6. (a) Simplified scheme of the crystal field splitting. (b) Experimental XAS data for 30 u.c. thick films (top panel) compared with the calculation in Mn^{3+} $L_{2,3}$ absorption (bottom panel). (c) Experimental LD data for the same film (top panel) compared with the calculation (bottom panel). Calculated data are obtained with $10Dq=1.1$ eV, $Ds=0.186$ eV, and $Dt=0.030$ eV (Ref. 11).

change peak, associated with the fast hopping of the $3d$ electrons among Mn ions in the metallic ferromagnetic regions, shows up as a sharp peak in the 370–400 MHz range. The spectral position of the localized Mn^{3+} states in manganites may be positioned, by theoretical considerations, in
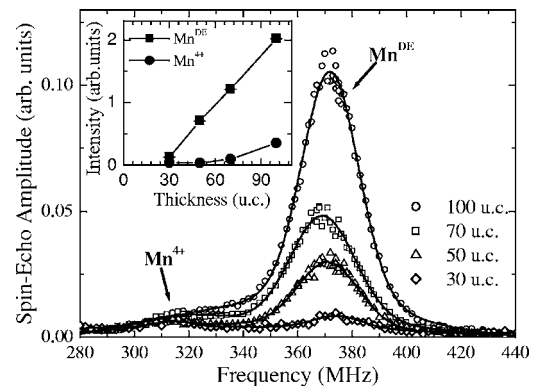

FIG. 7. Low temperature ($T=1.7$ K) NMR spectra for films of different thickness. The Mn^{DE} and Mn^{4+} peaks are indicated. The behavior of the integrated intensity of the two peaks as a function of temperature is shown in the inset.

250–490 MHz range.[21] Two distinct lines are observed in the experimental NMR spectra of Fig. 7 at 318 and 380 MHz, corresponding to Mn^{4+} and Mn^{DE} in the metallic ferromagnetic phase, respectively. The absence of a well resolved peak from localized Mn^{3+} in our spectra, in agreement with spectra reported by other researchers,[22] could be ascribed to its much faster relaxation rate and to a possibly larger spectral width. In the inset of Fig. 7 we report the integrated intensity of the two lines. It can be noticed that the intensity of the Mn^{DE} peak decreases linearly with the thickness, extrapolating to zero just below 30 u.c., whereas the intensity decrease of the Mn^{4+} line is marginal, compared to the former. As a consequence, in the case of the 30 u.c. thick film, the two intensities become comparable. From NMR measurements we can conclude, in agreement with resistivity measurements, that the local minimum state of the 30 u.c. film is nonmetallic while in the case of thicker films, for T approaching 0 K, we still have a sizeable contribution from the ferromagnetic metallic phase.

IV. DISCUSSION

First, we notice that the experimental findings illustrated in this paper cannot be explained on the basis of different physical effects such as intrinsic interface effects, cation nonstoichiometry, and oxygen deficiency. As a matter of fact, LSMO films grown, in the same conditions, on a better matched substrate such as (110) NdGaO$_3$ and (100) SrTiO$_3$, show a fully ferromagnetic/metallic behavior already for a thickness slightly larger than 10 u.c. Therefore, phenomena described in the present paper must be ascribed principally to the in-plane compressive epitaxial strain induced by the LAO substrate. The ferromagnetic metallic phase of manganites is in the orbital-disordered state. As a consequence, no dichroic signal is expected in the XAS spectra. On the contrary, the LD spectra of thin LSMO films grown on a LAO substrate indicate a preferential occupation of the out-of-plane $3z^2-r^2$ orbitals.[11] Such orbital ordering is a fingerprint of the C-type antiferromagnetic (AF) insulating phase. The stabilization of the $3z^2-r^2$ orbitals is a consequence of the in-plane compressive tetragonal distortion induced by the epitaxial strain, which increases the Mn-O bond length along the out-of-plane direction.[10,11] Such an interpretation of the LD spectra is strongly supported by XAS-LD measurements carried out on various AF orbital ordered manganites of different compositions, including La$_{1-x}$Sr$_{1+x}$MnO$_4$ layered manganites.[12,23] For instance, a remarkable agreement can be noticed between the experimental LD spectra of the LaSrMnO$_4$ layered manganite[12] (which exhibits a C-type AF $3z^2-r^2$ ordering) and our fully strained LSMO film (Fig. 8). Once more, while the shape of the LD spectra is remarkably similar, a difference can be noticed in the amplitude of the LD signals, which is larger in the case of layered manganites relative to the fully strained film on LAO. The experimental behavior of LSMO films under different strain conditions can be explained on the basis of the experimental phase diagram proposed by Konishi and co-workers,[9] and then explained theoretically by Fang and co-workers.[24] In Fig. 9 we report the phase diagram of La$_{1-x}$Sr$_x$MnO$_3$, c/a ratio versus doping
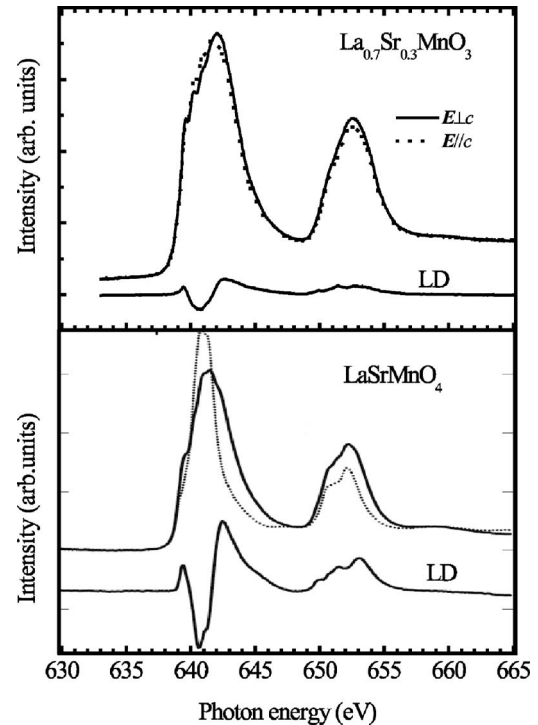

FIG. 8. LD and XAS measurements taken with the electric E vector perpendicular (V polarization) and E parallel (H polarization) to the film c axis of the 30 u.c. thick LSMO film (upper panel) compared with the data reported in literature on a LaSrMnO$_4$ sample (lower panel, adapted from Ref. 12).

x (figure adapted from Refs. 20 and 24). Full dots represents our set of samples. According to this phase diagram, the fully strained 30 u.c. thick film ($c/a=1.06$) lies in the C-type AF ground state stability region, while partially relaxed films lay in the F ground state stability region, though close to the phase coexistence line. However, experimental LD spectra at room temperature show that the transition from the C-type AF to F phase is not abrupt (Fig. 5). On the contrary, contribution from the $3z^2-r^2C$ phase increases gradually as the c/a ratio increases. Such a finding seems indicative of phase coexistence between the $3z^2-r^2$ C phase and the orbital dis-
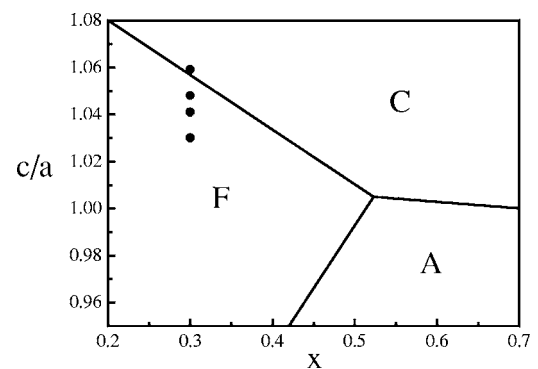

FIG. 9. Phase diagram of La$_{1-x}$Sr$_x$MnO$_3$ (adapted from Refs. 20 and 24). c/a represents the ratio between the perpendicular and the in-plane lattice parameter of the film. The full dots at $x=0.3$ indicate our LSMO films on LAO substrate having different thickness.

ordered F phase, with the concentration ratio between the two phases controlled by the c/a strain parameter. The co-existence of the two phases can also explain the lower amplitude of the LD signal of our films compared with the layered manganites, which are fully C-type orbitally ordered (Fig. 8). LD results are in agreement with the transport measurements reported in Fig. 4, which show a decrease of the metal-insulator transition temperature as the thickness is decreased from 100 to 30 u.c. Variations of the intensity of the LD signal can be tentatively ascribed to the occurrence of nanometric phase separation between C-type AF insulating phase and the F metallic phase.[11] Phase separation on a nanometric scale has been experimentally proved by scanning tunnel spectroscopy in the case of both $La_{0.7}Sr_{0.3}MnO_3$ and $La_{0.7}Ca_{0.3}MnO_3$ films.[5,6] In the present case phase separation can be enhanced by the proximity to the phase separation line (Fig. 9). Overall the experimental behavior described in this paper can be understood on the basis of a nanocluster separation phenomenon which starts to occur at a temperature T^* higher than the mean field ordering temperatures.[3] Phase separation is driven by the epitaxial strain in the proximity of the transition line between C-type AF and F phases. Strain can modify the relative amount of the two phases in the mixed composition region as deduced from the intensity of the LD signal. However, even in the case of the fully strained film, the disordered F phase is not completely suppressed and the intensity of the LD signal is lower than that expected for a fully ordered $3z^2-r^2$ AF phase. When decreasing the temperature, domains of the energetically less favored phase start to reduce. Consequently, resistivity undergoes a percolative metal-insulator transition at T_P equal to 275 and 250 K for 70 u.c. ($c/a=1.04$) and 50 u.c. ($c/a=1.045$) thick films, respectively. On the contrary, the fully strained film (30 u.c., $c/a=1.06$), which is in the C-type AF stability region, shows an insulating behavior with no metal-insulator transition in the whole temperature range. A further ingredient is added by the low temperature NMR measurements. In agreement with the above scenario the fully strained film, in the insulating state, shows only a marginal Mn^{DE} contribution in the NMR spectrum, whereas the spectrum of the nearly relaxed film, in the metallic state, is dominated by the Mn^{DE} peak (Fig. 7). However, all our films show a Mn^{4+} peak, whose relative weight increases with increasing the strain, indicating the presence of an additional ferromagnetic insulating (FI) component from the bulk of the film, similar to that measured in LSMO and $La_{2/3}Ca_{1/3}MnO_3$ films grown on $SrTiO_3$.[13,14] In bulk materials this component is characterized by x^2-y^2 orbital occupation, which, according to the semiempirical Goodenough-Kanamori-Anderson rules,[25] introduces ferromagnetic interactions between Mn^{3+} and Mn^{4+}. Hence the FI component that we detect cannot be directly responsible for the sign of the detected average LD signal, but its further presence within the insulating layers contributes to reduce the intensity of the LD signal. This third component should be explicitly considered in future inhomogeneous models including the effects of disorder as those of Ref. 2. The whole set of physical measurements reported in this paper could be understood in the framework of a scenario which foresees competing phases in the presence of substantial disorder. In this case a gap region can
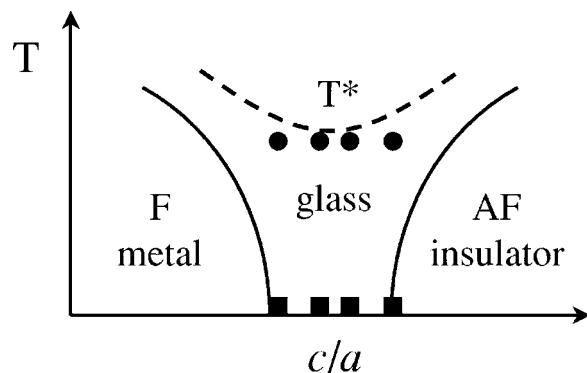

FIG. 10. Schematic phase diagram (adapted from Ref. 2). Representative points of our films are tentatively reported as full dots at room temperature and full squares at low temperature.

open between the stable phases. States in this region have glassy characteristics and consist of coexisting clusters of the two phases.[1] This scenario is summarized in Fig. 10, which has been adapted from Ref. 2. In this schematic phase diagram the representative points of our strained LSMO films have been tentatively reported.

V. CONCLUSION

LSMO thin films having different thickness were grown by PLD with *in situ* RHEED diagnostics on LAO substrates in a 2D layer-by-layer mode. Mismatch between film and substrate gives rise to an in-plane compressive biaxial strain which can be carefully measured by XRD. For our growth conditions, partial relaxation of epitaxial strain occurs in the case of films whose thickness exceeds 30 u.c. and consequently the c/a ratio varies from 1.06 to 1.03. In-plane compressive strain induces an elongation of the out-of-plane Mn-O bonds. This effect results in the stabilization of the $3z^2-r^2$ orbitals, thus giving rise to a sizeable XAS-LD signal. The shape of the LD signal varies weakly with the c/a ratio, while its intensity strongly increases with c/a. At the same time, resistivity increases and the metal-insulator transition shifts toward lower temperatures until reaching an insulating state for the fully strained 30 u.c. thick film. Low temperature NMR spectra show a decrease of the Mn^{DE} contribution, which becomes negligible in the 30 u.c. thick film and an additional contribution of ferromagnetic Mn^{4+} from a minority FI component. The theoretical simulation of XAS-LD is in qualitative agreement with the experimental results. The contribution of the Mn^{4+} ions and the coexistence of the orbital ordered and disordered phases can explain the relative intensity of the dichroic signal, which is smaller than the value expected for a fully ordered $3z^2-r^2$ sample. The whole set of physical measurements reported in this paper can be understood in the framework of strain driven competing phases in the presence of disorder.[2] In this scenario a gap region, having glassy characteristics, can open between the stable phases. For intermediate values of the epitaxial strain, the local minimum state of the system lies in this

region and consists of coexisting clusters of AF and *F* phases, plus a minority contribution from a FI phase. In conclusion, by only changing the thickness of the film we induce a gradual variation of the strain strength, monitored by the c/a ratio. Such a parameter is used as a driving force to span the glassy region. Orbital ordering and Mn^{DE}/Mn^{4+} contributions are monitored across the glassy region. A gradual variation of the relative amount of the two AF and *F* phases with changing the strain has been demonstrated.

*Electronic address: carmela.aruta@uniroma2.it

[1] E. Dagotto, New J. Phys. **7**, 67 (2005).

[2] E. Dagotto, Science **309**, 257 (2005).

[3] J. Burgy, M. Mayr, V. Martin-Mayor, A. Moreo, and E. Dagotto, Phys. Rev. Lett. **87**, 277202 (2001).

[4] J. Burgy, A. Moreo, and E. Dagotto, Phys. Rev. Lett. **92**, 097202 (2004).

[5] T. Becker, C. Streng, Y. Luo, V. Moshnyaga, B. Damaschke, N. Shannon, and K. Samwer, Phys. Rev. Lett. **89**, 237203 (2002).

[6] Amlan Biswas, M. Rajeswari, R. C. Srivastava, T. Venkatesan, R. L. Greene, Q. Lu, A. L. de Lozanne, and A. J. Millis, Phys. Rev. B **63**, 184424 (2001).

[7] Y. Murakami, J. H. Yoo, D. Shindo, T. Atou, and M. Kikuchi, Nature (London) **423**, 965 (2003).

[8] G. C. Milward, M. J. Calderon, and P. B. Littlewood, Nature (London) **433**, 607 (2005).

[9] Y. Konishi, Z. Fang, M. Izumi, T. Manako, M. Kasai, H. Kuwahara, M. Kawasaki, K. Terakura, and Y. Tokura, J. Phys. Soc. Jpn. **68**, 3790 (1999).

[10] N. M. Souza-Neto, A. Y. Ramos, H. C. N. Tolentino, E. Favre-Nicolin, and L. Ranno, Phys. Rev. B **70**, 174451 (2004).

[11] C. Aruta, G. Ghiringhelli, A. Tebano, N. G. Boggio, N. B. Brookes, P. G. Medaglia, and G. Balestrino, Phys. Rev. B **73**, 235121 (2006).

[12] D. J. Huang, W. B. Wu, G. Y. Guo, H.-J. Lin, T. Y. Hou, C. F. Chang, C. T. Chen, A. Fujimori, T. Kimura, H. B. Huang, A. Tanaka, and T. Jo, Phys. Rev. Lett. **92**, 087202 (2004).

[13] M. Bibes, Ll. Balcells, S. Valencia, J. Fontcuberta, M. Wojcik, E. Jedryka, and S. Nadolski, Phys. Rev. Lett. **87**, 067210 (2001).

[14] A. A. Sidorenko, G. Allodi, R. De Renzi, G. Balestrino, and M. Angeloni, Phys. Rev. B **73**, 054406 (2006).

[15] A. Tebano, N. G. Boggio, C. Aruta, B. Davidson, P. G. Medaglia, and G. Balestrino, Eur. Phys. J. B **51**, 337 (2006).

[16] J. Chavanne, P. Van Vaerenbergh, P. Elleaume, and T. Gunzel (unpublished).

[17] G. Allodi, A. Banderini, R. De Renzi, and C. Vignali, Rev. Sci. Instrum. **76**, 083911 (2005).

[18] A. M. Haghiri-Gosnet, J. Wolfman, B. Mercey, Ch. Simon, P. Lecoeur, M. Korzenski, M. Hervieu, R. Desfeux, and G. Baldinozzi, J. Appl. Phys. **88**, 4257 (2000); A. Yu. Petrov, C. Aruta, S. Mercone, C. Adamo, I. Alessandri, and L. Maritato, Eur. Phys. J. B **40**, 11 (2004).

[19] R. D. Cowan, *The Theory of Atomic Structure and Spectra* (University of California Press, Berkeley, 1981).

[20] Y. Tokura and N. Nagaosa, Science **288**, 462 (2000).

[21] A. J. Freeman and R. E. Watson, in *Magnetism*, edited by G. T. Rado and H. Suhl (Academic, New York, 1965), Vol. IIA, p. 168.

[22] M. M. Savosta, V. N. Krivoruchko, I. A. Danielenko, V. Y. Tarenkov, T. E. Konstantinova, A. V. Borodin, and V. N. Varyukhin, Phys. Rev. B **69**, 024413 (2004).

[23] W. B. Wu, D. J. Huang, G. Y. Guo, H.-J Lin, T. Y. Hou, C. F. Chang, C. T. Chen, A. Fujimori, T. Kimura, H. B. Huang, A. Tanaka, and T. Jo, J. Electron Spectrosc. Relat. Phenom. **137**, 641 (2004).

[24] Z. Fang, I. V. Solovyev, and K. Terakura, Phys. Rev. Lett. **84**, 3169 (2000); Z. Fang and K. Terakura, J. Phys. Soc. Jpn. **70**, 3356 (2001).

[25] See, for example, J. B. Goodenough, Phys. Rev. **100**, 564 (1955); J. J. Kanamori, J. Phys. Chem. Solids **10**, 87 (1959); P. W. Anderson, in *Magnetism*, edited by G. T. Rado and H. Suhl (Academic Press, New York, 1963), Vol. 1, Chap. 2.